International Journal of Innovative Computing, Information and Control
Volume **8**, Number **12**, December **2012**

 ISSN 1349-4198
pp. 8089–8102

POWER-ASSISTED WHEELCHAIR DESIGN BASED ON A LYAPUNOV TORQUE OBSERVER

Chin-Chih Ou and Tien-Chi Chen

Department of Engineering Science
National Cheng Kung University
No. 1, University Road, Tainan City 701, Taiwan
ou@mail.ksu.edu.tw; tienchi@gmail.com

Received August 2011; revised December 2011

Abstract. *The objective of this paper is to present, describe and experimentally verify a novel sensorless power-assisted wheelchair (PAWC) of significantly lower cost and higher performance than contemporary designs. The proposed PAWC is built around a torque observer using the Lyapunov stability theorem. The design is essentially sensorless, having only two conventional commercial opticoupler speed sensors, one for each of the two pulse width modulated motors. The only other input is voltage feedback produced by the motor drivers. The novel adaptive torque observer estimates the impact torque and predicts the system state, outputting a control signal for a proportional-integral controller through a digital signal processor. Experiments were conducted by simulation and also with a lab-built prototype to verify that the proposed method has good performance and meets the requirements for safe and stable PAWC design. Also, the proposed torque observer is found more accurate than a conventional torque observer. Because the proposed sensorless PAWC demonstrates better performance, lower intrinsic cost and superior maintenance probability than conventional PAWCs, the presented system is a likely candidate for the next-generation of PAWCs.*
Keywords: Power-assisted wheelchair, Torque observer, Lyapunov stability theorem

1. **Introduction.** The average human life span is lengthening and the average human birth rate is declining. As a result, elderly persons are becoming a larger percentage of the human population. Together with other temporary and permanent human handicap conditions, this is helping drive development of various mechatronic assists for physically compromised people. Accordingly, important developments are occurring in the fields of robotic and power-assisted adjuncts for the human body [1-6]. Traditionally, users unable to propel themselves in a manual wheelchair are pushed by a human assistant [6]. More recently, researchers have focused on medically related electric vehicles such as fully powered wheelchairs [7]. However, the optimal rehabilitation of the aged or convalescent requires a therapeutically modulated regimen of rest and exercise, which cannot be supplied by conventional wheel chair systems, powered or unpowered. Manual wheelchairs have an efficiency of between 5% and 18% [8,9] and tend to induce upper extremity joint degeneration, with injury incidence between 25% and 80% [10,11]. Thus, wheelchair designers have developed alternatives such as lever drives and crank drives requiring exercise and active coordination of the user [12,13]. Relatively recently, a new class of wheelchair known as the power-assisted wheelchair (PAWC), has appeared. Representing a hybrid between manually and electrically powered wheelchairs, a PAWC combines human and robotic abilities whereby a mechatronic system detects and amplifies the force applied by the human user. Electro-hydraulic and electric power assist systems are common in power-assisted steering for many vehicles [3-6]. Similar electric power assist systems

are now being applied to drive PAWCs [1,2]. PAWC devices are increasingly critical in a world containing a progressively higher percentage of elderly citizens. Fully powered wheel chairs/vehicles fail to provide the physical exercise and practical coordination that is required for optimal medical rehabilitation of the patient. Thus, PAWC's have come into being. Early PAWCs converted push rim force into an electronic control input by use of linear compression springs which manipulated a simple potentiometer. Present commercial PAWC designs use a variety of different sensors, including multi-directional accelerometers, electronic gyroscopes and advanced pressure sensors mounted on the push rim. The use of multiple sensors complicates the electro-mechanical control task, increases system cost, design complexity, system size and weight and also increases the risk of component failure.

The PAWC proposed in this study uses what is commonly called a "sensorless" type of torque observer. In actual fact, the present design employs two opticoupler encoders (sensors), one on each of the two electric motors. These sensors measure the motors' speed and direction. Such opticoupler sensors are commonly available as factory-available add-ons with electric motors. Opticoupler sensors are inexpensive, extremely reliable and interface easily with digital systems. A load torque observer is similar to differentiator for a low-frequency signal. Load torque measurement in traditional PAWCs generally requires additional sensors of complex varieties [14], but sensorless approaches have also been attempted. One example is the Luenberger observer, though this is a complicated design that must set mathematical poles and add a gain to trace system torque [15,16]. Another PAWC control method uses physiological feedback from the wheelchair user to help control the wheelchair, but such systems require additional devices for physiological detection, as well as having significant design and implementation issues [18,19]. Chen and Ho proposed a torque observer based on a neural network employing a complex weight calculation method [23]. Katsura and Ohnishi presented torque estimation based on a linear mechanical model, but they failed to consider coupling between the wheels [2]. Choi et al. used a conventional linear observer employing the pole assignment method to design the observer gain [26].

To overcome these problems, this paper presents a PAWC using a sensorless (excepting the two aforementioned opticouplers), simple and effective high-order torque observer that employs the Lyapunov stability theorem to determine observer gain and system stability. The proposed adaptive torque observer is used in conjunction with a simple proportional-integral (PI) controller that modulates the contribution of two common electric motors. The adaptive torque observer estimates the impact torque of the wheelchair. The PI controller accelerates convergence with the trace targets. Experimental results below will show that the proposed method has high performance and is suitable for PAWC design. Moreover, the proposed observer measurements are more accurate than those of a conventional load torque observer [19]. Finally, the proposed PAWC design is of lighter weight, lower cost, is easier to design and implement and has a higher probability functional reliability than conventional PAWCs.

2. **Wheelchair Hardware.**

The wheelchair main body is an A&I WCFF182S/1 (A&I, Taiwan), which is a manually powered lightweight aluminum-frame wheelchair typical of contemporary design (Figures 1 and 2). Power assist is implemented by adding two conventional 24V DC motors (M29SGX-B2-2418, Xajong, Taiwan) with reduction gearing transmission attachments (Figure 3). Motor speed and direction are detected by two inexpensive commercial optocoupler encoders (model IRS 320, Sumtak), one for each motor. A flat toothed belt connects the small motor pulley to a larger pulley mounted on the axel

just inside the wheelchair's unmodified wheels, one belt for each motor. Belts are used because they are inexpensive, tolerant of axial alignment, require minimal maintenance, are intrinsically quiet, damp vibration and have high power transmission efficiency (90-98%). The two gear pulleys together multiply the motor force applied to the wheel by more than 5 times. Figure 4 details the small gear pulley, large gear pulley and transmission belt.

Two conventional 12V lead/acid gel cells supply power to the system. These two batteries are connected in series, giving the total system a 24V DC power supply. Highdensity lithium batteries are a possible but more expensive alternative to the lead/acid option. Each of the two motors achieves its own torque magnitude and rotational direction via its own driver circuit. The motors/drivers employ the power-efficient pulse width modulation (PWM) technique, so only a single-sided DC power source is required. The responses of the motors/drivers are much faster than the dynamic response of the mechanical system. The PWM driver is a conventional circuit consisting of four power transistors. Upon

FIGURE 1. Power-assisted wheelchair body

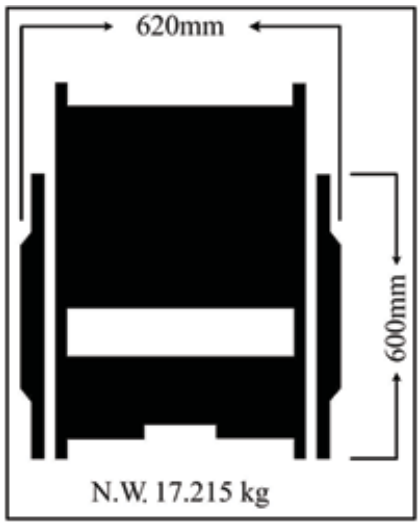

FIGURE 2. Experimental wheelchair overall dimensions

FIGURE 3. Motors, reduction gear and belt linkage to wheel

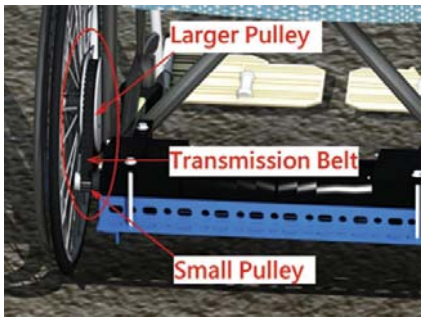

FIGURE 4. Detail of toothed pulleys and transmission belt

receiving a suitable control input, the driver stimulates the DC motor to rotate in a clockwise or counter-clockwise direction. The motor's direction is determined by the control signal i^*, which also sets the magnitude of the torque. The closer that i^* approaches a value of 1.65V, the smaller is the magnitude of the torque. At a control input of 1.65V, the motor is motionless. The largest torque is activated by either 0V or 3.33V. Equivalent voltage values greater or less than 1.65V produce equivalent torque but drive the motor in the opposite direction. The electronic control system is a lab-built circuit board based on a Texas Instruments digital signal processing (DSP) chip (TMS320F/C2407, Figure 5).

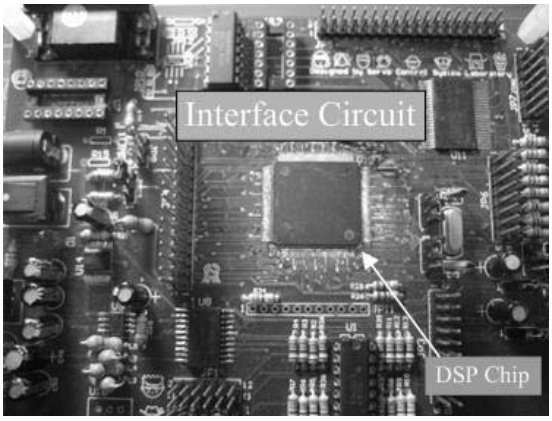

FIGURE 5. DSP chip and interface circuit board

3. **Wheelchair Model.** To simplify the wheelchair kinematic model, this study does not consider the wheelchair's passive front wheels. According to kinematic theory, the push force f and torque T on a wheelchair rim can be expressed as

$$f = M\ddot{x} = Mr\ddot{\theta} \tag{1}$$

$$T = I\alpha = Mr^2\ddot{\theta} \tag{2}$$

where $\ddot{\theta}$, r, M, I and α represent the angular acceleration velocity of the wheel, wheel radius, wheelchair body mass, moment of inertia and angular acceleration of the body, respectively.

According to Equations (1) and (2), the thrust f the left wheel motor's electromagnetic torque T_{eL} and the right wheel motor's electromagnetic torque T_{eR} can be expressed as

$$f = M_c r\ddot{\theta} + m_w r\ddot{\theta}_{f_L} + m_w r\ddot{\theta}_{f_R} \tag{3}$$

$$T_{eL} = m_w r^2\ddot{\theta}_{tL} + m_c r^2\left(\frac{\ddot{\theta}_{tL}}{2}\right) \tag{4}$$

$$T_{eR} = m_w r^2\ddot{\theta}_{tR} + m_c r^2\left(\frac{\ddot{\theta}_{tR}}{2}\right) \tag{5}$$

where M_c is the mass of the wheelchair body without wheels, m_w and r are the mass and radius of the wheels respectively, $\ddot{\theta}_{f_L}$ is the user-generated push-force angular acceleration of the left wheel, $\ddot{\theta}_{f_R}$ is the user-generated push-force angular acceleration of the right wheel, $\ddot{\theta}_{tL}$ is the left wheel's motorgenerated angular acceleration and $\ddot{\theta}_{tR}$ is the right wheel's motor-generated angular acceleration.

Laplace transform of Equations (3)-(5) leads to

$$\begin{aligned} f &= M_c r s^2\theta + m_w r s^2\theta_{f_L} + m_w r s^2\theta_{f_R} \\ &= \frac{M_c r + 2m_w r}{2} s\omega_{f_L} + \frac{M_c r + 2m_w r}{2} s\omega_{f_R} \end{aligned} \tag{6}$$

$$T_{eL} = \frac{m_c r^2 + 2m_w r^2}{2} s\omega_{tL} \tag{7}$$

$$T_{eR} = \frac{m_c r^2 + 2m_w r^2}{2} s\omega_{tR} \tag{8}$$

According to Equations (6)-(8), the left force f_L and right force f_R can be expressed as

$$f_L = \frac{M_c r + 2m_w r}{2} s\omega_{f_L} \tag{9}$$

$$f_R = \frac{M_c r + 2m_w r}{2} s\omega_{f_R} \tag{10}$$

The angular velocity of both side driving wheels can be expressed as

$$\omega_L = \omega_{f_L} + \omega_{tL} \tag{11}$$

$$\omega_R = \omega_{f_R} + \omega_{tR} \tag{12}$$

where ω_{f_L} and ω_{f_R} respectively represent the velocity of the left and right wheels produced by the push force f, while ω_{tL} and ω_{tR} respectively represent the velocity of the left and right wheels produced by the motor. Only the left wheel will be discussed herein because the situation and configuration are the same for both the left and right wheels.

Assuming that the wheelchair is moving on level ground and the wheels on both sides are the same, then the state equation for the left wheel can be expressed as

$$\begin{bmatrix} \dot{\omega}_L \\ \dot{i}_a \end{bmatrix} = \begin{bmatrix} \frac{-2B}{(M_c+2m_w)r^2} & \frac{2K_t}{(M_c+2m_w)r^2} \\ \frac{-K_e}{L_a} & \frac{-R_a}{L_a} \end{bmatrix} \begin{bmatrix} \omega_L \\ i_a \end{bmatrix} + \begin{bmatrix} \frac{2}{(M_c+2m_w)r^2} \\ 0 \end{bmatrix} T_{lL} + \begin{bmatrix} 0 \\ \frac{1}{L_a} \end{bmatrix} v_s \tag{13}$$

$$y = \begin{bmatrix} 1 & 1 \end{bmatrix} \begin{bmatrix} \omega_L \\ i_a \end{bmatrix} \tag{14}$$

where the state variables ω_L and i_a are the state speed of the left wheel and DC motor state current, respectively. T_{lL} is the push wheel torque, R_a and L_a are respectively the armature resistance and inductance, K_e and K_t are respectively the back emf and torque constant, while M, r and B are respectively the wheelchair mass, wheel radius and friction constant.

The state i_a is easy to obtain, so the adaptive torque observer expression can be reduced as

$$\begin{aligned} \dot{\hat{\omega}}_L = &\begin{bmatrix} \frac{-2B}{(M_c+2m_w)r^2} & \frac{2K_t}{(M_c+2m_w)r^2} \end{bmatrix} \begin{bmatrix} \hat{\omega}_L \\ i_a \end{bmatrix} \\ &+ \frac{2}{(M_c + 2m_w) r^2} \hat{T}_{lL} + k_1(\hat{\omega}_L - \omega_L) \end{aligned} \tag{15}$$

where $\hat{\omega}_L$, i_a and $\hat{T}_{lL}$ respectively represent the estimated state speed of the left wheel, state armature current and estimated push wheel torque.

The load torque estimation is defined as

$$\hat{T}_{lL} = k_i \int (\hat{\omega}_L - \omega_L)dt + k_p(\hat{\omega}_L - \omega_L) \tag{16}$$

where k_i and k_p are the PI controller gains for accelerated estimation of the wheelchair load torque. Further,

$$v_s = \int k_{ii}(i_a^* - i_a)dt + k_{pp}(i_a^* - i_a) \tag{17}$$

$$T_e = i_a K_t \tag{18}$$

$$T_e^* = \hat{T}_{lL} G \tag{19}$$

where k_{ii} and k_{pp} are accelerated constant gains and T_e, T_e^* and G are the actual motor electromagnetic torque, the motor electromagnetic torque command and the power assist ratio, respectively.

According to the above formula, the control algorithm for the proposed system is expressed as follows:

Step 1: Calculate the speed of the left wheel ω_L and DC motor current i_a for a push wheel torque T_{lL} using Equations (13) and (14).
Step 2: Calculate the estimated speed of the left wheel $\hat{\omega}_L$ using Equation (15).
Step 3: Calculate load torque estimation $\hat{T}_{lL}$ using Equation (16).
Step 4: Calculate motor electromagnetic torque command T_e^* using Equation (19).
Step 5: Calculate DC motor current command using $i_a^* = T_e^*/K_t$.
Step 6: Calculate v_s using Equation (17). Return to Step 1.

4. **Torque Observer Design Using Lyapunov Stability Theorem.** Figure 6 shows a block diagram of the proposed system. Whereas a conventional torque observer considers "disturbance torque" the proposed torque observer considers T_{lL}, i.e., the power torque in terms of the user hand thrust force multiplied by the wheel radius. Defining $e_\omega = (\hat{\omega}_L - \omega_L)$ and $e_{TL} = (\hat{T}_{lL} - T_{lL})$, then Equations (12) and (13) can be rewritten as

$$\dot{e}_\omega = A_{11} \cdot e_\omega + B_1 \cdot e_{TL} + k_1 \cdot e_\omega \tag{20}$$

$$\dot{e}_{TL} = -k_p \dot{e}_\omega - k_i e_\omega \tag{21}$$

where $A_{11} = -2B/[(M_c+2m_w)r^2]$, $A_{12} = 2K_t/[(M_c+2m_w)r^2]$ and $B_1 = 2/[(M_c+2m_w)]r^2$.

In practice, the observer gain affects system stability. The system convergence rate will be too slow under a low gain, resulting negligible power-assist effect at low speed [14]. In

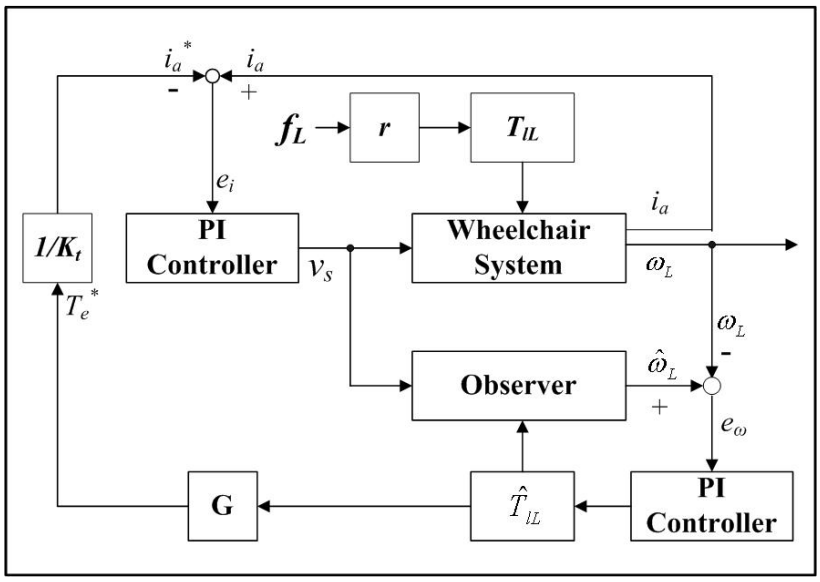

FIGURE 6. Block diagram of PAWC with adaptive observer

contrast, if G is set too large, the PAWC wheel will accelerate too fast and the user will not be able to maintain physical hand contact with the push rim, presenting a danger to the user [20]. The system will also be prone to vibration and instability.

Accordingly, this study applies Lyapunov stability theory to the torque observer design to ensure system stability. The Lyapunov function V is chosen as

$$V = \frac{1}{2}e_{\omega}^2 + \frac{1}{2}e_{TL}^2 \tag{22}$$

The derivative of the Lyapunov function V can be expressed as

$$\dot{V} = e_{\omega} \cdot \dot{e}_{\omega} + e_{TL} \cdot \dot{e}_{TL} \tag{23}$$

Substituting Equations (20) and (21) into Equation (23) yields

$$\begin{aligned} \dot{V} &= e_{\omega}\dot{e}_{\omega} + e_{TL}\dot{e}_{TL} \\ &= e_{\omega}(A_{11} + B_1 e_{TL} + K_1 e_{\omega}) + e_{TL}(-k_p\dot{e}_{\omega})(-k_i e_{\omega}) \\ &= (A_{11} + k_1)e_{\omega}^2 + (B_1 - A_{11}k_p - k_1 k_p - k_i)e_{TL}e_{\omega} - k_p B_1 e_{TL}^2 \end{aligned} \tag{24}$$

To comply with the Lyapunov stability theorem, $\dot{V}$ must be negative to guarantee observer stability.

Thus

$$\dot{V} = (A_{11} + k_1)e_{\omega}^2 + (B_1 - A_{11}k_p - k_1 k_p - k_i)e_{TL}e_{\omega} - k_p B_1 e_{TL}^2 < 0 \tag{25}$$

In obtaining $\dot{V}$, it is important that the third term in Equation (25) be originally negative. If the first and second terms become negative, then $\dot{V}$ will be negative. Because the e_{TL} and e_{ω} terms cannot be ensured negative or positive, let the second term be zero. Let the first term be negative to ensure that the square of e_{ω} is positive. The two-term equation can be ordered as

$$B_1 - A_{11}k_p - k_1 k_p - k_i = 0 \tag{26}$$

$$A_{11} + k_1 < 0 \tag{27}$$

$$k_p B_1 > 0 \tag{28}$$

In Equations (26)-(28), the observer and PI controller gain can be deduced as

$$k_i = B_1 - A_{11}k_p - k_1 k_p \tag{29}$$

$$k_1 < -A_{11} \tag{30}$$

$$k_p > 0 \tag{31}$$

5. **Computer Simulations and Experimental Results.** This study evaluates and verifies the proposed system using both computer simulation and a lab-built experimental PAWC. Opticoupler encoder data is used as an objective measure of the speed of the wheel, from which the actual impact torque is computed conventionally. The presented system employing the Lyapunov stability theorem is compared with an identical mechatronic system employing a traditional torque observer design that is well represented in the literature [21]. The prototype hardware includes two identical systems, one for each wheel. Each system includes one of the following (i.e., two total in the combined dual system): a conventional permanent magnet motor, a PWM driver and a lab-built circuit board. Each circuit board contains a peripheral component interface (PCI) with a DSP. Figure 7 shows the general structure of the experimental PAWC prototype The parameters of the PAWC are summarized as: $M_c = 80$Kg, $m_w = 2$Kg, $r = 0.3$m, $B = 0.1$Kgms/rad, $R_a = 1.2\Omega$, $L_a = 8.6\text{e}{-3}$mH, $K_t = 0.5$Kgm/A, $K_b = 0.0319$vs/rad, $f_d = 0.00012$Kgms/rad and $J = 0.00003\text{Kgm}^2$.

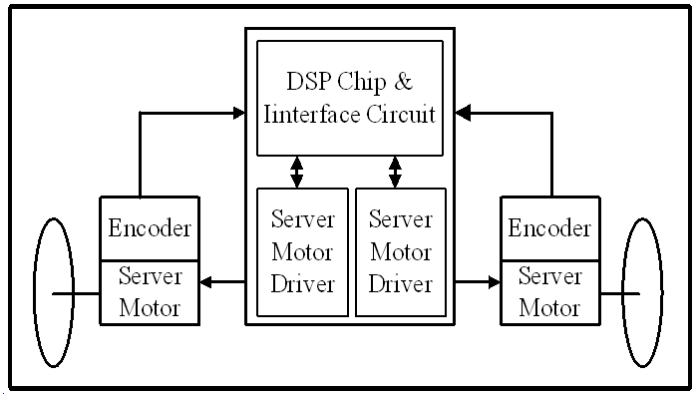

FIGURE 7. General structure of the prototype PAWC

As in a normal manual wheelchair, the speed of the PAWC is controlled by the torque applied to the wheels' push rims by the user's arms. When the user manually applies force to the PAWC's wheels, the proposed control system treats the resulting impact torque as a command to define the PAWC's thrust. The system then multiplies this torque by the assist ratio, where the assist ratio gain is G. The assist ratio cannot be fixed. If G is set too large, the PAWC wheel will accelerate too fast and the user will not be able to maintain physical hand contact with the push rim, presenting a danger to the user [20]. Conversely, if G is set too small, the power-assist effect will be negligible at low speed [14]. Therefore, the proposed controller adapts G appropriately to the thrust of the user. G is determined experimentally during the design stage of the system. In general, the G is expressed as

$$G = \begin{cases} 10 \times 3^{-N\hat{T}_{lL}} + 1 & \text{when } \hat{T}_{lL} > 0 \\ 10 \times 3^{N\hat{T}_{lL}} + 1 & \text{when } \hat{T}_{lL} < 0 \end{cases}, \tag{32}$$

where the optimum N depends on the user's physiological condition and preferences, but is suggested herein to lie between about $1 \sim 3$. Further, in future commercial systems, G probably can be refined by the user and/or the therapist.

6. **Computer Simulation.** Because PAWC operation can have serious consequences regarding the physical safety of the user, a computer simulation was run prior to practical experiments. Figures 8 to 13 present the results of various relevant computer simulations. Figure 8 shows a computer simulation of the actual impact torque T_{lL} applied by the user to the left wheel and the observed impact torque $\hat{T}_{lL}$ of the left wheel using the proposed adaptive observer. This figure reveals that the observed impact torque is very close to the actual impact torque for the presented system. Figure 9 presents a computer simulation showing the actual impact torque T_{lL} and observed impact torque $\hat{T}_{lL}$ using the traditional torque observer. Comparison of Figures 8 and 9 shows that the proposed observer's ability to track torque is faster than that of the traditional observer. Figure 10 shows a computer simulation for the left wheel speed ω_L and the observed left wheel speed $\hat{\omega}_L$, confirming that the proposed system observes the left wheel speed rapidly and tracks the wheel speed tightly. Figure 11 shows the computer simulation for the impact torque $\hat{T}_{lL}$ observed by the proposed system and resulting torque command T_e^*, where T_e^* represents the torque that is added to the PAWC wheel. Remember that PAWC users need a control system that does not "overcontrol", i.e., avoids sudden bursts of power which might overbalance the user. Thus, a sudden moment of impact torque from the user should not cause a sudden burst of power from the power assist system. Figure 11

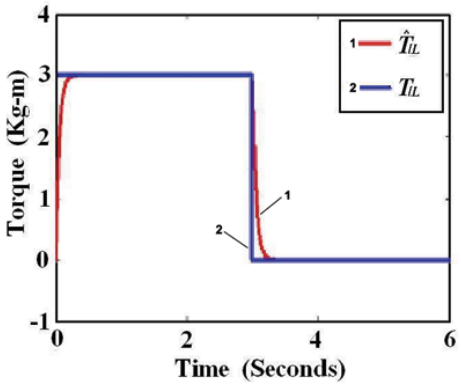

FIGURE 8. Computer simulated actual impact torque T_{lL} and observed impact torque $\hat{T}_{lL}$ of left wheel using the proposed torque observer

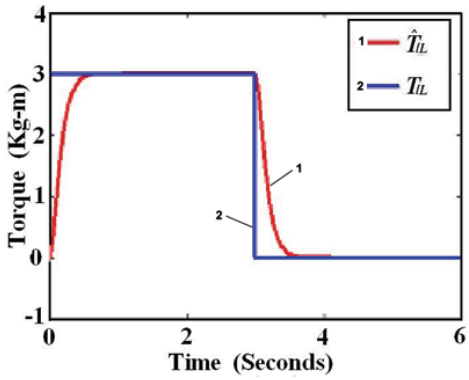

FIGURE 9. Computer simulated impact torque T_{lL} and observed impact torque $\hat{T}_{lL}$ of left wheel using the traditional torque observer

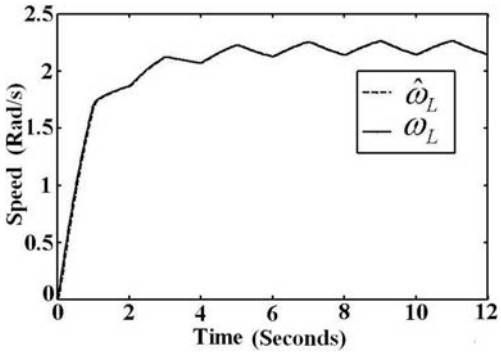

FIGURE 10. Computer simulated actual left wheel speed ω_L and observed left wheel speed $\hat{\omega}_L$

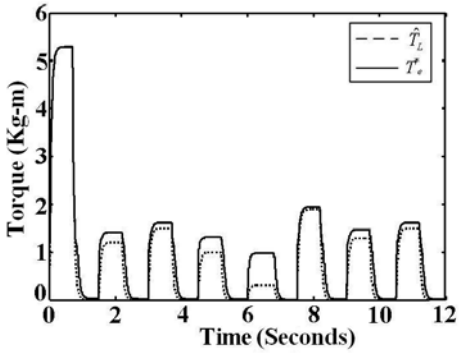

FIGURE 11. Computer simulated results for observed impact torque $\hat{T}_{lL}$ compared with the power-assisted torque T_e^* added to the PAWC

shows that when $\hat{T}_{lL}$ is large, the system multiplies the input torque by a smaller multiple of G so that T_e^* remains at a safe and reasonable output level, thereby maintaining system stability. When $\hat{T}_{lL}$ is small, the full force is multiplied by a larger multiple of G so that T_e^* increases significantly, allowing a small impact torque to produce significant power assist.

As in all motive systems with independently powered wheels, accurate coordination of the wheels is critical for safe and reliable operation. When moving in a circle, a wheelchair requires thrust torque on one wheel alone and no thrust on the other wheel. Figure 12 shows a computer simulation of the dynamic trajectory of the PAWC while moving in a circle, indicating that the proposed torque observer/controller meets the requirements quitewell. Similarly, when moving in a straight line, both independent power-assisted wheels must produce equal thrust torque on both wheels. Figure 13 shows a computer simulation of the dynamic trajectory of the PAWC for straight ahead movement. When both hands exert the same impact torque, the dynamic trajectory produces a straight line.

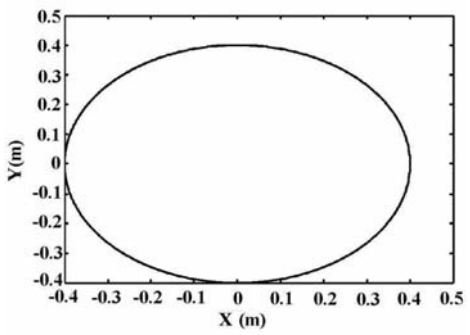

FIGURE 12. Computer simulated results for the dynamic trajectory of the PAWC while moving in a circle

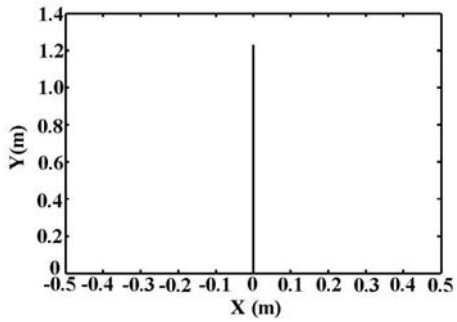

FIGURE 13. Computer simulated results for the dynamic trajectory of the PAWC for straight ahead movement

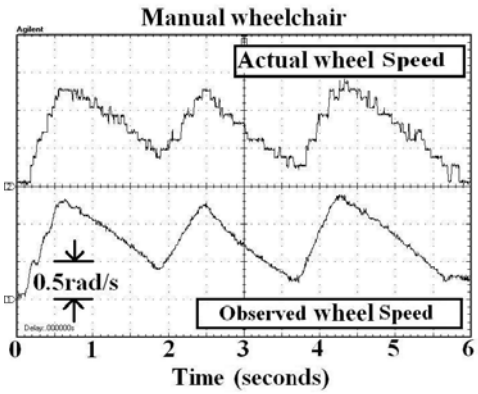

FIGURE 14. Experimental results for the manual wheelchair's actual wheel speed and observed wheel speed

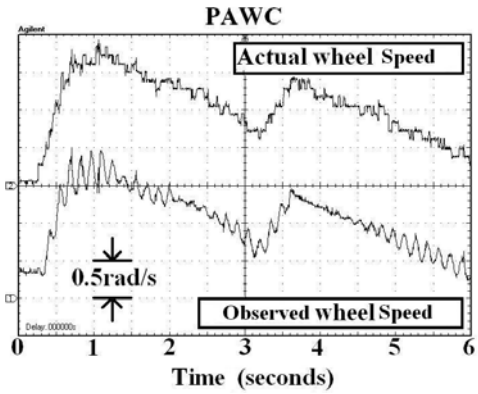

FIGURE 15. Experimental results for PAWC's actual wheel speed and observed wheel speed

7. **Experimental Results.** After successful computer simulation, the laboratory prototype was tested in real-time experiment on the flat laboratory floor by a normal healthy user. First, the unpowered (manual) power-assisted wheelchair's actual left wheel speed and observed wheel speed were observed while the user's two hands applied periodic torque to the push rims (Figure 14). The experimental results confirm that the observed wheel speed tightly tracks the actual wheel speed. Next, Figure 15 shows the actual and observed left wheel's speed of the fully powered and operational PAWC when propelled by the same user. Again, it is seen that the actual and observed wheels speed match well, though the observed wheel speed is seen to exhibit a measurement oscillation around the actual wheel speed. This is an artifact of the power-assist input to the wheel and the system's compensation for brief moments of over/under power. In actual fact, this oscillation behavior is unnoticeable to the user. In both of the experimentally measured waveforms of Figures 14 and 15, the observer estimated speed $\hat{\omega}_L$ and the actual measured speed ω_L match each other closely during two-handed continuous propulsion.

Figure 16 shows the experimental results for the PAWC's actual impact torque T_{lL} and the observed impact torque $\hat{T}_{lL}$ of the left wheel. This figure reveals that even when different forces pass through Equation (32), the proposed control scheme yields the same

net torque assist, thereby assuring system stability and user security. Note that in Figure 16, the PAWC is allowed to come to a full stop between instances of applied torque. Figure 17 shows the PAWC when propelled by periodic two-handed user thrust. The initial performance is in approximately straight forward motion. Figures 17(a) and 17(b) show the human-applied thrust torque and the power-assisted electromagnetic torque applied to the PAWC's left and right wheels, respectively. Figures 17(c) and 17(d) show the armature current command i_a_command and the actual armature current i_a of the PAWC's left and right wheels, respectively. Figure 17(e) shows the speed of both the left and right wheels during a period of slight directional deviation. The opticoupler speed encoder detects the

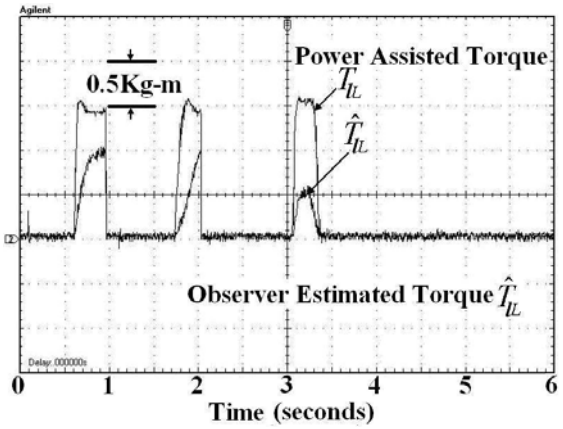

FIGURE 16. Experimental results for actual power-assisted torque T_{lL} and observed estimated torque $\hat{T}_{lL}$ of the PAWC's left wheel using the proposed adaptive observer

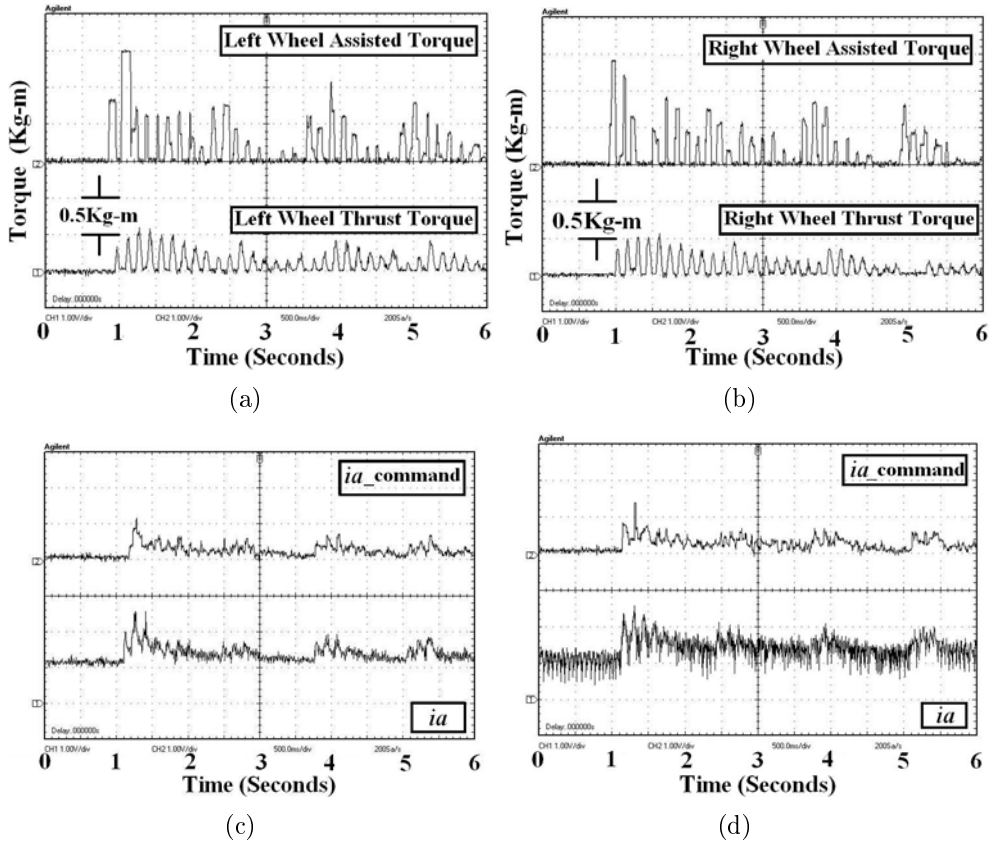

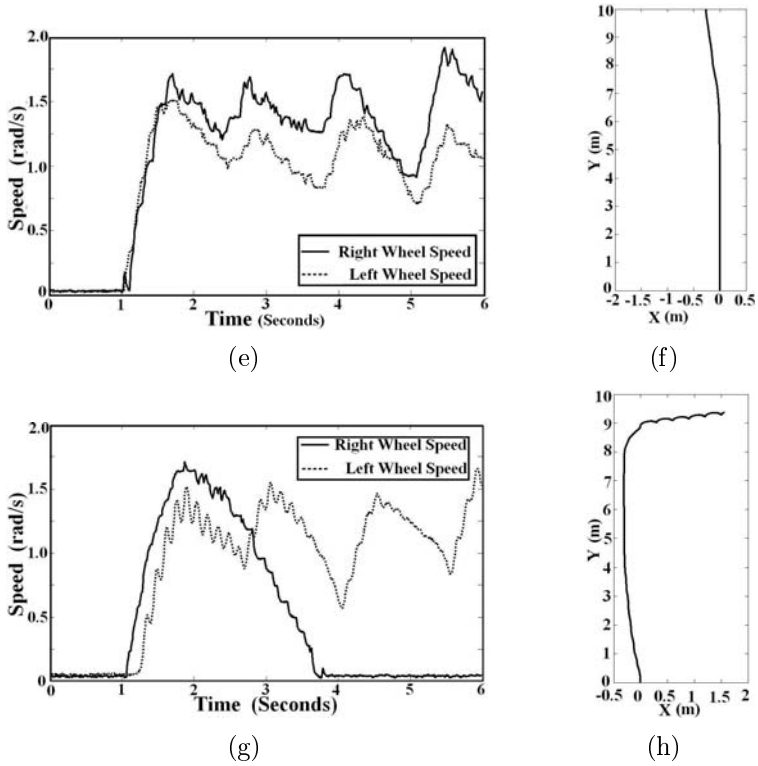

FIGURE 17. PAWC experimental results with straight trajectory and turn: (a) human thrust torque and assisted torque of the left wheel; (b) human thrust torque and assisted torque of the right wheel; (c) armature current command and armature current i_a of the left wheel; (d) armature current command and armature current i_a of the right wheel; (e) left and right PAWC wheel speeds while moving approximately straight; (f) straight forward trajectory of the PAWC, with the user deviating slightly toward the left after 6m; (g) left and right wheel speeds of the PAWC during a right turn and (h) right turn trajectory of the PAWC

wheel speed and passes it to the algorithm to obtain the armature command current, which then commands the system to produce a power-assisted torque that assists generation of the final wheelchair speed. Figures 17(a) and 17(b) show the actual human thrust which, via the proposed control system, results in the additional behaviors seen in Figures 17(a)-17(e). If the PAWC starts to move with low user-generated torque, then the power-assisted torque must be larger. Inspection of the figures confirms that this desired behavior appears in the resulting power-assisted behavior, i.e., the proposed PAWC moves with a level of power-assisted torque suitable to the user's requirements/commands. Figure 17(f) shows the approximately straight trajectory of the PAWC, confirming stable compliance with the manual commands of the user. Notably, the user starts to veer to the left after proceeding approximately 6 meters, but the trajectory is completely stable. Figure 17(g) shows the speeds of the left and right wheels of the PAWC as the user performs a strong right turn. Figure 17(h) shows the net right turn trajectory of the presented PAWC as the user performs a strong right turn after a period of forward progress. Overall, it is seen that the proposed PAWC complies effectively with user commands, without stutter or balk.

Consideration of the experimental results displayed in these figures confirms the essential functionality of the proposed PAWC. These abilities combined with the lower cost,

easier design, higher probability of long-term utility and superior performance relative to a PAWC controlled by a traditional torque observer confirm the presented PAWC design as a likely candidate for the next generation of commercial PAWCs.

8. **Conclusion.** This study has presented an improved power-assisted wheelchair that allows wheelchair users to avoid the excessive arm, shoulder pain and damage caused by traditional hand push wheelchairs. Further, the presented PAWC encourages optimal rehabilitation of aged/convalescent users by requiring the patient's active physical coordination and exercise, which is not supplied by conventional fully powered wheel chair systems. Previous PAWC designs use complex sensor systems or control algorithms which increase system cost, system complexity, design difficulties and probability of system failure. The proposed design is what is commonly known as "sensorless"; nevertheless, the proposed system uses two inexpensive and intrinsically reliable optical speed encoders (one for each motor) such as those that are normally included in speedcritical electric motors. The only other input to the controller is the backvoltage of the motor drivers. The presented design combines an adaptive observer and a PI controller to precisely control the PAWC. Because safety is a critical PAWC requirement, the proposed design uses a torque observer based on the Lyapunov stability theorem to estimate the impact torque, compute the needed power assist and accurately control the system. Computer simulated results show that the presented system has superior performance compared with a popular and traditional torque observer design. Real-time experimental results using a lab-built prototype confirm that the observed impact torque, stator current and wheel speed accurately and rapidly track the actual values, providing safety and comfort for the user. Because the proposed sensorless PAWC system demonstrates good performance and because of its low intrinsic cost, ease of design and high probability of mechatronic longevity, it is a likely candidate for the next generation of commercial PAWCs. Our group's future research on this topic will investigate "sensorless" sensing of physiological tremor in the user's arms for detection, diagnosis and compensation of user fatigue; integrating wireless networking capabilities for patient tracking, monitoring and telemedicine options.

REFERENCES

[1] L. Silva, T. Felzer, G. Neto, R. Nordmann and F. Dedini, Modeling a hands-free controlled power wheelchair, *Lecture Notes in Computer Science*, vol.5105, pp.1261-1268, 2008.

[2] S. Katsura and K. Ohnishi, Human cooperative wheelchair for haptic interaction based on dual compliance control, *IEEE Trans. Ind. Electronics*, vol.51, no.1, pp.221-228, 2004.

[3] D. Ding and R. A. Cooper, Electric powered wheelchairs, *IEEE Control Syst. Mag.*, vol.25, no.2, pp.22-34, 2005

[4] T. Yasuda, K. Nakamura, A. Kawahara and K. Tanaka, Neural network with variable type connection weights for autonomous obstacle avoidance on a prototype of six-wheel type intelligent wheelchair, *International Journal of Innovative Computing, Information and Control*, vol.2, no.5, pp.1165-1177, 2006.

[5] M. Athanasiou and J. Clark, A Bayesian network model for the diagnosis of the caring procedure for wheelchair users with spinal injury, *Comput. Meth. and Programs in Biomedicine*, vol.95, no.2, pp.S44-S54, 2009.

[6] K.-L. Su, S.-H. Chia, J.-H. Guo and B.-Y. Li, Develop a power predictive system for scheduling loading of mobile robots, *ICIC Express Letters*, vol.5, no.8(B), pp.2791-2798, 2011.

[7] M. Nash, D. Koppens, M. V. Haaren, A. Sherman, J. Lippiatt and J. Lewis, Power-assisted wheels ease energy costs and perceptual responses to wheelchair propulsion in persons with shoulder pain and spinal cord injury, *Arch. Phys. Med. Rehabil.*, vol.89, pp.2080-2085, 2008.

[8] P. Giacobbi, C. Levy, F. Dietrich, S. Winkler, M. Tillman and J. Chow, Wheelchair users' perceptions of and experiences with power assist wheels, *Am. J. Phys. Med. Rehabil.*, vol.89, no.3, pp.225-234, 2010.

[9] H. Lakomy, I. Campbell and C. Williams, Treadmill performance and selected physiological characteristics of wheelchair athletes, *Br. J. Sports Med.*, vol.21, no.3, pp.130-133, 1987.
[10] R. Glaser, M. Sawka, L. Laubach and A. Suryaprasad, Metabolic and cardiopulmonary responses to wheelchair and bicycle ergometry, *J. Appl. Physiol.*, vol.46, no.6, pp.1066-1070, 1979.
[11] R. Cooper, T. Corfman, S. Fitzgerald, M. Boninger, D. Spaeth, W. Ammer and J. Arva, Performance assessment of a pushrim-activated power-assisted wheelchair control system, *IEEE Trans. Control Syst. Technol.*, vol.10, no.1, pp.121-126, 2002.
[12] H. Gellman, D. Chandler, J. Petrasek, I. Sie, R. Adkins and R. Waters, Carpal tunnel syndrome in paraplegic patients, *J. Bone Joint Surg.*, vol.70, no.4, pp.517-519, 1988.
[13] P. Nichols, P. Norman and J. Ennis, Wheelchair user's shoulder? Shoulder pain in patients with spinal cord lesions, *Scand J. Rehabil Med.*, vol.11, no.1, pp.29-32, 1979.
[14] L. van der Woude, E. Botden, I. Vriend and H. Veeger, Mechanical advantage in wheelchair lever propulsion: Effect on physical strain and efficiency, *J. Rehabil. Res. Dev.*, vol.34, no.3, pp.286-289, 1997.
[15] R. Cooper, S. Fitzgerald, M. Boninger, K. Prins, A. Rentschler, J. Arva and T. O'Connor, Evaluation of a push rim-activated, power-assisted wheelchair, *Arch. Phys. Med. Rehabil.*, vol.82, no.5, pp.702-708, 2001.
[16] A. Kakimoto, H. Matsuda and Y. Sekiguchi, Development of power-assisted attendant-propelled wheelchair, *Int. J. Jpn. Soc. Precis Eng.*, vol.65, no.8, pp.1126-1130, 1999.
[17] Y. Liu and Z. Wang, A prediction-based data collection method in wireless sensor network using Kalman filter, *ICIC Express Letters, Part B: Applications*, vol.2, no.6, pp.1439-1446, 2011.
[18] L. Yao and Y.-S. Chen, A type-2 fuzzy controller for automatic guided vehicle wall-following control, *ICIC Express Letters, Part B: Applications*, vol.1, no.1, pp.77-83, 2010.
[19] A. Takahashi and R. Oguro, Torque and speed estimation with parameter identification of line-start induction motor operated value, *International Journal of Innovative Computing, Information and Control*, vol.5, no.12(A), pp.4551-4559, 2009.
[20] H.-S. Chuang, Y.-C. Chuang and C.-Y. Chen, Development of two-quadrant PMDC motor drives with regenerative braking on electric vehicles, *ICIC Express Letters*, vol.5, no.9(B), pp.3321-3328, 2011.
[21] D. Luenberger, An introduction of observer, *IEEE Trans. Autom. Control*, vol.16, no.6, pp.596-602, 1971.
[22] B. Shafai, C. Pi, S. Nork and S. Linder, Proportional integral adaptive observer for parameter and disturbance estimations, *IEEE Trans. Ind. Electronic*, vol.4, no.1, pp.4694-4699, 2002.
[23] H. J. Ho and T. C. Chen, Motorized CPM/CAM physiotherapy device with sliding-mode fuzzy neural network control loop, *Comput. Meth. Programs Biomed.*, vol.96, pp.96-107, 2009.
[24] R. Cooper, T. Fletcher-Shaw and R. Robertson, Model reference adaptive control of heart rate during wheelchair ergometry, *IEEE Trans. Control Syst. Technol.*, vol.6, no.4, pp.507-514, 1998.
[25] Y. Oonishi, O. Sehoon and Y. Hori, A new control method for power-assisted wheelchair based on the surface myoelectric signal, *IEEE Trans. Ind. Electron.*, vol.57, no.9, pp.3191-3196, 2010.
[26] S. Choi, J. Ko, I. Kim, J. Park and S. Hong, Precise position control using a PMSM with a disturbance observer containing a system parameter compensator, *Proc. of Electric Power Appl.*, vol.152, no.6, pp.1573-1577, 2005.
[27] N. Li, Y. Han and C. He, Capacitive sensor design for an automatic car-wiper system, *ICIC Express Letters, Part B: Applications*, vol.2, no.4, pp.879-884, 2011.
[28] L. C. Shiu, C. Y. Lee and C. S. Yang, Obstacle-free robot deployment algorithm for wireless sensor networks, *ICIC Express Letters, Part B: Applications*, vol.2, no.2, pp.325-330, 2011.
[29] S. Zhang, G. Wu and S. Zheng, Speed following driver model based on self-adaptive chaotic genetic PID and preview control, *ICIC Express Letters*, vol.5, no.11, pp.4041-4046, 2011.
[30] T. J. Ren and T. C. Chen, Modeling and control of a power-assisted mobile vehicle based on torque observer, *IET Control Theory Appl.*, vol.1, no.5, pp.1405-1412, 2007.